Radiative and Optical Properties of $La_{1-x}Sr_xMnO_3$ $(0 \le x \le 0.4)$ in the Vicinity of Metal-Insulator Transition Temperatures from 173 to 413K[1]

K. Shimazaki[2], S. Tachikawa[3], A. Ohnishi[3] and Y. Nagasaka[4, 5]

[1] Paper presented at Fourteenth Symposium on Thermophysical Properties, June 25-30, 2000, Boulder, Colorado, U.S.A.

[2] Graduate School of Science and Technology, Keio University, 3-14-1, Hiyoshi, Yokohama, 223-8522, Japan.

[3] The Institute of Space and Astronautical Science, 3-1-1, Yoshinodai, Sagamihara, 229-8510, Japan.

[4] Department of System Design Engineering, Keio University, 3-14-1, Hiyoshi, Yokohama, 223-8522, Japan

[5] To whom correspondence should be addressed.

ABSTRACT

Radiative and optical properties of polycrystalline $La_{1-x}Sr_xMnO_3$ $(0 \le x \le 0.4)$ in the vicinity of metal-insulator transition are presented. Temperature dependence of the total hemispherical emittance ε_H of $La_{1-x}Sr_xMnO_3$ was measured by calorimetric method in the temperature range from 173 to 413K. It was confirmed that the ε_H showed unexpected variations result from difference of hole concentration (x). Especially in the case of $La_{0.825}Sr_{0.175}MnO_3$, ε_H keeps high value above transition temperature T_C due to insulator-like behavior; on the other hand, it decreases sharply below T_C because of metallic behavior. Spectral reflectance was measured by FT-IR in the wavelength range of 0.25 to 100μm at room temperature. Optical constants were calculated from Kramers-Kronig analysis of the spectral reflectance data. Insulator-like feature of the optical properties appears at lower Sr^{2+} doping level while metallic one exists at higher Sr^{2+} doping level.

KEY WORDS: Kramers-Kronig analysis; $La_{1-x}Sr_xMnO_3$; manganese oxide; optical constants; perovskite; spectral reflectance; total hemispherical emittance.

1. INTRODUCTION

In order to keep the desired temperature of the spacecraft for all mission phases, a wide variety of thermal control materials or devices have been used. It is recently required to develop new thermal control materials for spacecraft because of the tendency to grow higher density and efficiency of the instruments on the spacecraft. It is important to know the thermal radiative and optical properties of such newly developed thermal control materials. As a new thermal control material, we employed $La_{1-x}Sr_xMnO_3$ which is manganese oxide with a perovskite-type structure $LaMnO_3$ by substitution of La^{3+} sites with Sr^{2+}. These perovskite-type manganites have attracted much attention on account of their phenomenal magnetic and transport properties. Especially giant magnetoresistance phenomena and metal-insulator transition have been widely observed as long as the Mn^{4+}/Mn^{3+} mixed valence ratio is in the appropriate range [1-3]. The mechanism of the ferromagnetic transition and the coincident metal-insulator transition has been traditionally understood on the basis of the double exchange interaction model [4-7]. Later, recent theoretical and experimental studies pointed out the importance of electron-phonon interaction, called a "polaron", that relates to Jahn-Teller-type lattice distortions of MnO_6 octahedra [8, 9] in addition to double exchange interaction.

Here we present the radiative and optical properties of $La_{1-x}Sr_xMnO_3$ in the vicinity of metal-insulator transition temperatures. They show various changes depending on its temperature and molar ratio of Sr^{2+}. Temperature dependence of the total hemispherical emittance ε_H was measured by the calorimetric method between 173K and 413K. Spectral reflectance was measured by FT-IR in the wavelength range of 0.25 to 100μm at room temperature so as to investigate the influence of Sr^{2+} doping

level on the optical properties. The optical constants, refractive index n and extinction coefficient k, which subject radiative and optical properties were calculated from Kramers-Kronig (K-K) analysis of the spectral reflectance data. Absorption coefficient A was calculated by the use of k.

2. INVESTIGATED SAMPLES AND CHARACTERIZATION

Polycrystalline $La_{1-x}Sr_xMnO_3$ (x=0, 0.15, 0.175, 0.2, 0.3 and 0.4) were selected as test samples and prepared using the standard ceramic production process [10]. The dimensions of the sample are nearly 30mm×30mm×0.2mm. The surfaces of every sample were polished by diamond slurry. The surface roughness of the sample was measured by surface roughness measuring instrument (Tokyo Seimitsu CO., LTD.: SURFCOM 130A). The root-mean-square roughness of the sample was under 30nm.

As the hole concentration (x) is increased, $La_{1-x}Sr_xMnO_3$ shows any phase changes [3]. The parent material $LaMnO_3$ is an antiferromagnetic insulator. For doping levels $0.1 \le x \le 0.17$, the phase changes from paramagnetic insulator to ferromagnetic insulator state with decreasing temperature. The ferromagnetic metal phase appears over $x \approx 0.17$ and the ferromagnetic transition temperature T_C exists near room temperature. Namely, rapid reduction of electronic resistivity begins at T_C and metal phase turns up at low temperature, it is so-called a metal-insulator transition. And over $x \approx 0.25$, the phase changes from paramagnetic metal to ferromagnetic metal state as the temperature is reduced. Hence, it is speculated that the radiative and optical properties of $La_{1-x}Sr_xMnO_3$ shows considerable variations in the vicinity of metal-insulator transition.

3. TOTAL HAMISPHERICAL EMITTANCE ε_H

Total hemispherical emittance ε_H was measured by the calorimetric method. A detailed explanation of the calorimetric method and description of the measurement system will be published elsewhere [11]. The uncertainty of the present ε_H measurement was estimated to be at most ±2.5%.

Figure 1 shows the result obtained in the present measurement on ε_H of $La_{1-x}Sr_xMnO_3$ (x=0, 0.15, 0.175, 0.2, 0.3 and 0.4) in the temperature range from 173 to 413K. Temperature dependence of ε_H in $La_{1-x}Sr_xMnO_3$ shows distinct behavior with doping level of Sr^{2+}. $LaMnO_3$ is an insulator and does not show any phase changes in this temperature range [3]. Hence, no drastic change can be observed and ε_H shows monotonous increase as a function of temperature. For x=0.15, ε_H keeps constant above 250K and slightly changes with paramagnetic-ferromagnetic insulator transition below 250K [3]. The similar result is obtained between x=0.175 and x=0.2 though the transition temperature and sharpness of the variation of ε_H are little different. The result indicates the unconventional features for thermal radiative properties of these samples. Namely on one hand ε_H keeps high value above T_C due to insulator-like behavior; on the other hand, it decreases sharply below T_C because of metallic behavior. The amount of variation of ε_H is over 0.40. These anomalous behaviors of ε_H for x=0.175 and 0.2 are ascribed to the great change of the infrared reflectance because the phonon structures in infrared region fade away by dielectric screening effect resulted from increasing mobility of free electrons with metal-insulator transition [12, 13]. For x=0.3 and 0.4, the inclinations of the temperature dependence of ε_H slightly varies with the paramagnetic-ferromagnetic transition [3]. The ε_H of x=0.3 and 0.4 is

smaller than the other samples in the entire temperature range due to metallic state over the whole temperature region.

Figure 2 shows the measured ε_H of $La_{1-x}Sr_xMnO_3$ (x=0, 0.15, 0.175, 0.2, 0.3 and 0.4) at 293K. The effect of Sr^{2+} doping on the ε_H is clearly appeared. The ε_H is obviously different between $0 \le x \le 0.175$ and $0.175 \le x \le 0.4$. In the vicinity of x=0.175 which is close to the nonmetal-metal compositional phase boundary [1], ε_H shows remarkably variation according to slightly difference of Sr^{2+} doping. When the doping level is small, ε_H has large value as well as nonmetal. As high doping level at which the mobility of the free electrons increase, the ε_H becomes gradually small and closes to the value like metal. The reason of doping dependence in ε_H at room temperature will be discussed in section 4.3.

4. OPTICAL PROPERTIES

4.1. Experimental and Kramers-Kronig Analysis

Spectral reflectance of near-normal incidence was measured for $La_{1-x}Sr_xMnO_3$ (x=0, 0.15, 0.175, 0.2, 0.3 and 0.4) at room temperature. Spectral reflectance in the wavelength region of 0.25~100μm was measured using Fourier-transform spectroscopy (Bio-Rad: FTS-60A/896). As a reference, we used aluminum mirror. The optical constants, refractive index *n* and extinction coefficient *k*, were calculated from Kramers-Kronig (K-K) analysis [14] of the spectral reflectance data. At near-normal incident angle, *n* and *k* are given by

$$n = \frac{1-R}{1+R-2\sqrt{R}\cos\theta} \tag{1}$$

$$k = \frac{-2\sqrt{R}\sin\theta}{1+R-2\sqrt{R}\cos\theta} \tag{2}$$

where the quantity R is the experimentally observed spectral reflectance (single surface reflection). The n, k and R are functions of frequencies, which is omitted to simplify the expressions in eqs. (1) and (2). The phase difference θ between the incident and the reflected waves is obtained from the following relation.

$$\theta(\omega_i) = -\frac{\omega_i}{\pi}\int_0^\infty \frac{\ln[R(\omega)/R(\omega_i)]}{\omega^2-\omega_i^2}d\omega \tag{3}$$

Here, $\theta(\omega_i)$ is the value of the phase difference at frequency ω_i. The integral is evaluated numerically. Extrapolations of the spectral reflectance to high and low frequencies are required since the measured spectral range is finite. For the analysis we assumed the constant reflectance from 0.25 to 0.1μm and $R \propto \omega^{-4}$ extrapolation below 0.1μm. Depending on the electronic states, the reflectance extrapolations above 100μm were the constant reflectance or the reflectance described by Hagen-Rubens relation $(1-R) \propto \sqrt{\omega}$. Absorption coefficient is given by [15]

$$A = \frac{4\pi}{\lambda}k \tag{4}$$

where λ is a wavelength.

4.2. Assessment of the Data Calculated from K-K Analysis

To investigate the K-K analysis error due to the uncertainty in the extrapolation of the spectral reflectance from zero to infinity, we perform analytical dispersion analysis of the measured spectral reflectance. A model based on the following factorized expression of the complex dielectric function is applied [16]:

$$\hat{\varepsilon}(\omega) = \varepsilon_1 + i\varepsilon_2 = \varepsilon_\infty \prod_j \frac{\omega^2 - \omega_{Tj}^2 + i\gamma_{Tj}\omega}{\omega^2 - \omega_{Lj}^2 + i\gamma_{Lj}\omega} \tag{5}$$

The adjustable parameters, the high-frequency dielectric constant ε_∞, the frequencies ω_{Tj}, ω_{Lj} and damping terms γ_{Tj}, γ_{Lj} for *j*th transverse optical (TO)-longitudinal optical (LO) pair, are uniquely determined. And then, ε_1 and ε_2 are real and imaginary part of the complex dielectric constants, respectively. The band contour described by the factorized model is similar to that by the classical analytical model for the complex dielectric constant. The model has been successfully used to fit infrared spectral reflectance of several oxidic perovskite [17, 18]. The factorized model has four free parameters per oscillator instead of three as in the classical model, so it is much more flexible than the classical model.

The spectral reflectance is expressed as eq. (6) by the use of the ε_1 and ε_2. We performed curve fitting with eqs. (5) and (6). A simplex method [19] is employed for curve fitting.

$$R = \frac{\sqrt{\left(\varepsilon_1^2 + \varepsilon_2^2\right)} - \sqrt{2\left(\varepsilon_1 + \sqrt{\varepsilon_1^2 + \varepsilon_2^2}\right)} + 1}{\sqrt{\left(\varepsilon_1^2 + \varepsilon_2^2\right)} + \sqrt{2\left(\varepsilon_1 + \sqrt{\varepsilon_1^2 + \varepsilon_2^2}\right)} + 1} \tag{6}$$

Representing $La_{1-x}Sr_xMnO_3$ system, the result of curve fitting to the spectral reflectance of $LaMnO_3$ is shown in Fig. 3. The open circles represent the measured spectral reflectance; solid curve is calculated by curve fitting. The fitting parameters obtained are listed in Table I. Little differences are observed near 30μm between measured spectral reflectance and fitted one. However, the factorized model satisfactorily describes the outline of the spectrum of $LaMnO_3$ and agrees well with measured reflectance. A standard deviation between measured spectral reflectance and fitted one is ±3.9%

The optical constants are expressed as eqs. (7) and (8) by the use of ε_1 and ε_2.

$$n = \sqrt{\frac{1}{2}\left(\sqrt{\varepsilon_1^2 + \varepsilon_2^2} + \varepsilon_1\right)} \tag{7}$$

$$k = \sqrt{\frac{1}{2}\left(\sqrt{\varepsilon_1^2 + \varepsilon_2^2} - \varepsilon_1\right)} \tag{8}$$

Good agreement between the optical constants that yield the best fit to reflectance data and those calculated from K-K analysis is observed as shown in Fig. 4. A standard deviation of the difference in optical constants obtained from K-K analysis and curve fitting is within ± 0.16. The result in wavelength region of 0.25~2.5μm and 80~100μm is omitted because it is unavoidable that the error is large by the nature of K-K analysis.

4.3. Spectral Reflectance

Figure 5 shows the measured spectral reflectance for $La_{1-x}Sr_xMnO_3$ (x=0, 0.15, 0.175, 0.2, 0.3 and 0.4) at room temperature. The distinct behaviors of the spectral reflectance are clearly observed. The spectral reflectance of x=0~0.175 shows up typical features of a nonmetal with sharp infrared peaks due to the transverse optical (TO) phonons at 17μm, 28 μm and 60 μm. A compound of the ideal cubic perovskite-type structure has three infrared-active phonon modes as shown in Fig. 6. Three strong TO phonon peaks correspond to Mn-O stretching mode, Mn-O-Mn bending mode and La-site external mode in the ascendant order of the wavelength [20, 21]. However, $LaMnO_3$ has more than three peaks in optical spectrum since $LaMnO_3$ is not ideal cubic but slightly distorted one. The Mn-O-Mn bending mode is most sensitive to the lattice distortion of MnO_6 octahedra [21].

Any notable distinction is not observed under 1.0μm though there are small

differences in magnitude of the spectral reflectance. Over 1.0μm, the spectral reflectance of x=0.3 and 0.4 is greatly different compared to that of x=0. With increasing Sr^{2+} doping, the optical phonon peaks gradually fade away and simultaneously the spectral reflectance becomes high in infrared region. Hence, two compounds of x=0.3 and 0.4 does not show insulator-like features in optical spectrum but metallic ones. It is considered that the reason why two compounds of x=0.3 and 0.4 have high reflectance is that there is a contribution to infrared optical phonon from free electrons which obtained more mobility due to Sr^{2+} doping. And then, free carriers contribution screens the infrared optical phonon mode [12, 13]. Consequently, the variation in ε_H at room temperature as shown in Fig. 2 is attributed to the variation in the infrared spectral reflectance due to Sr^{2+} doping.

4.4. Optical Constants and Absorption Coefficient

Figure 7 represents the optical constants calculated from K-K analysis. Wavelength dependence of the optical constants in x=0~0.2 is full of variety and there are three peaks though the bending mode of x=0 material is split due to lattice distortion. As Sr^{2+} doping increases, it is observed that three peaks gradually fade away as well as the spectral reflectance. In two compounds of x=0.3 and 0.4 that are metallic state at room temperature, the optical constants show metallic feature and monotonous increase as a function of the wavelength. The change from insulator-like behavior to metallic one in optical constants happens together with the change of spectral reflectance. The variation of the spectral reflectance is attributable to the metal-insulator transition due to Sr^{2+} doping in optical constants.

Absorption coefficient *A* obtained from eq. (4) is shown in Fig. 8. Like the

spectral reflectance and optical constants, the *A* varies from insulator-like feature to metallic one according to Sr^{2+} doping. The *A* of x=0.4 at 10μm is nearly two orders of magnitude larger than that of x=0. For insulator-like state, strong absorption peaks due to optical phonon are appeared at 17μm, 28 μm and 60 μm. In case of metallic state, obvious absorption peak is not observed and wavelength dependence is weak. From this result, at low doping level, it is verified that electromagnetic waves penetrate into materials to some extent depth from the surface and then absorbed by the optical phonon. On the other hand, at high doping level, electromagnetic waves are reflected at the surface or absorbed in relatively thin layer of the surface because it is hard for electromagnetic waves to penetrate due to free electrons contribution.

5. CONCLUSIONS

Temperature dependence of the total hemispherical emittance ε_H of $La_{1-x}Sr_xMnO_3$ system was confirmed in the temperature range from 173 to 413K. It was ascertained that ε_H showed variety changes by its temperature and Sr^{2+} doping. Moreover, the effect of Sr^{2+} doping on the optical properties was clarified. The optical constants were calculated from K-K analysis and the variation of the spectral reflectance is attributable to the metal-insulator transition due to Sr^{2+} doping in optical constants.

$La_{1-x}Sr_xMnO_3$ has potential for applications as thermal control material in space use because it has varied radiative and optical properties.

ACKNOWLEDGEMENTS

We would like to thank A. Okamoto, Y. Nakamura, Y. Shimakawa, M. Kosaka, T. Mori and A. Ochi of NEC Corporation for sample preparation.

REFERENCES

[1] Y. Tokura, A. Urushibara, Y. Moritomo, T. Arima, A. Asamitsu, G. Kido and N. Furukawa, *J. Phys. Soc. Jpn.* **63**: 3931 (1994).

[2] A. P. Ramirez, S. –W. Cheong and P. Schiffer, *J. Appl. Phys.* **81**: 5337 (1997).

[3] A. Urushibara, Y. Moritomo, T. Arima, A. Asamitsu, G. Kido and Y. Tokura, *Phys. Rev.* **51**: 14103 (1995).

[4] K. Kubo and N. Ohata, *J. Phys. Soc. Jpn.* **33**: 21 (1972).

[5] C. Zener, *Phys. Rev.* **81**: 403 (1951).

[6] P. –G. de Gennes, *Phys. Rev.* **118**: 141 (1960).

[7] P. W. Anderson and H. Hasegawa, *Phys. Rev.* **100**: 675 (1955).

[8] A. J. Millis, P. B. Littlewood and B. I. Shraiman, *Phys. Rev. Lett.* **74**: 5144 (1995).

[9] H. Y. Hwang, S. –W. Cheong, P. G. Radaelli, M. Marezio and B. Batlogg, *Phys. Rev. Lett.* **75**: 914 (1995).

[10] G. H. Jonker and J. H. van Santen, *Physica* **16**: 337 (1950).

[11] K. Shimazaki, S. Tachikawa, A. Ohnishi and Y. Nagasaka, *High Temp.-High Press.* (to be published).

[12] Y. Okimoto, T. Katsufuji, T. Ishikawa, A. Urushibara, T. Arima and Y. Tokura, *Phys. Rev. Lett.* **75**: 109 (1995).

[13] K. H. Kim, J. Y. Gu, H. S. Choi, G. W. Park and T. W. Noh, *Phys. Rev. Lett.* **77**: 1877 (1996).

[14] D. M. Roessler, *Brit. J. Appl. Phys.* **16**: 1119 (1965).

[15] R. Siegel and J. R. Howell, *Thermal Radiation Heat Transfer* 3rd ed. (Taylor&Francis, Washington, DC, 1992), pp. 524-525.

[16] D. W. Berreman and F. C. Unterwald, *Phys. Rev.* **174**: 791 (1968).

[17] K. Kamarás, K. –L. Barth, F. Keilmann, R. Henn, M. Reedyk, C. Thomsen, J. Kircher, P. Richards and J. –L. Stehlé, *J. Appl. Phys.* **78**: 1235 (1995).

[18] A. V. Boris, N. N. Kovaleva, A. V. Bazhenov, A. V. Samoilov, N. –C. Yen and R. P. Vasquez, *J. Appl. Phys.* **81**: 5756 (1997).

[19] J. A. Nelder and R. Mead, *Computer Journal* **7**, 308 (1965).

[20] K. Nakamoto, *Infrared and Raman Spectra of Inorganic and Coordiation Compounds*, 4th ed. (Wiley, New York, 1986), pp. 147-155.

[21] T. Arima and Y. Tokura, *J. Phys. Soc. Jpn.* **64**: 2488 (1995).

Table I. Fitting parameters determined by eqs. (5) and (6) for $LaMnO_3$.

j	1	2	3	4	5
ω_{Tj} (cm^{-1})	172.1	259.2	272.5	343.6	566.8
γ_{Tj}	13.7	53.4	31.6	43.4	28.8
ω_{Lj} (cm^{-1})	200.4	464.3	290.8	254.3	660.6
γ_{Lj}	10.1	50.1	34.2	42.8	41.4
ε_∞	6.6				

LIST OF FIGURE CAPTIONS

Fig. 1. Temperature dependence of total hemispherical emittance ε_H in $La_{1-x}Sr_xMnO_3$ (x=0, 0.15, 0.175, 0.2, 0.3 and 0.4).

Fig. 2. Total hemispherical emittance in $La_{1-x}Sr_xMnO_3$ (x=0, 0.15, 0.175, 0.2, 0.3 and 0.4) at 293K.

Fig. 3. Spectral reflectance of $LaMnO_3$. ○: measured data, —: the fitting curve of eqs. (6) and (7).

Fig. 4. Refractive index (a) and Extinction coefficient (b) of $LaMnO_3$. ○: calculated data from K-K analysis. —:calculated by eqs. (8) and (9) using the parameters in Table I.

Fig. 5. Spectral reflectance of $La_{1-x}Sr_xMnO_3$ (x=0, 0.15, 0.175, 0.2, 0.3 and 0.4) at room temperature.

Fig. 6. Infrared-active vibration modes of perovskite-type crystal structure.

Fig. 7. Refractive index (a) and extinction coefficient (b) of $La_{1-x}Sr_xMnO_3$ (x=0, 0.15, 0.175, 0.2, 0.3 and 0.4) at room temperature.

Fig. 8. Absorption coefficient of $La_{1-x}Sr_xMnO_3$ (x=0, 0.15, 0.175, 0.2, 0.3 and 0.4) at room temperature.

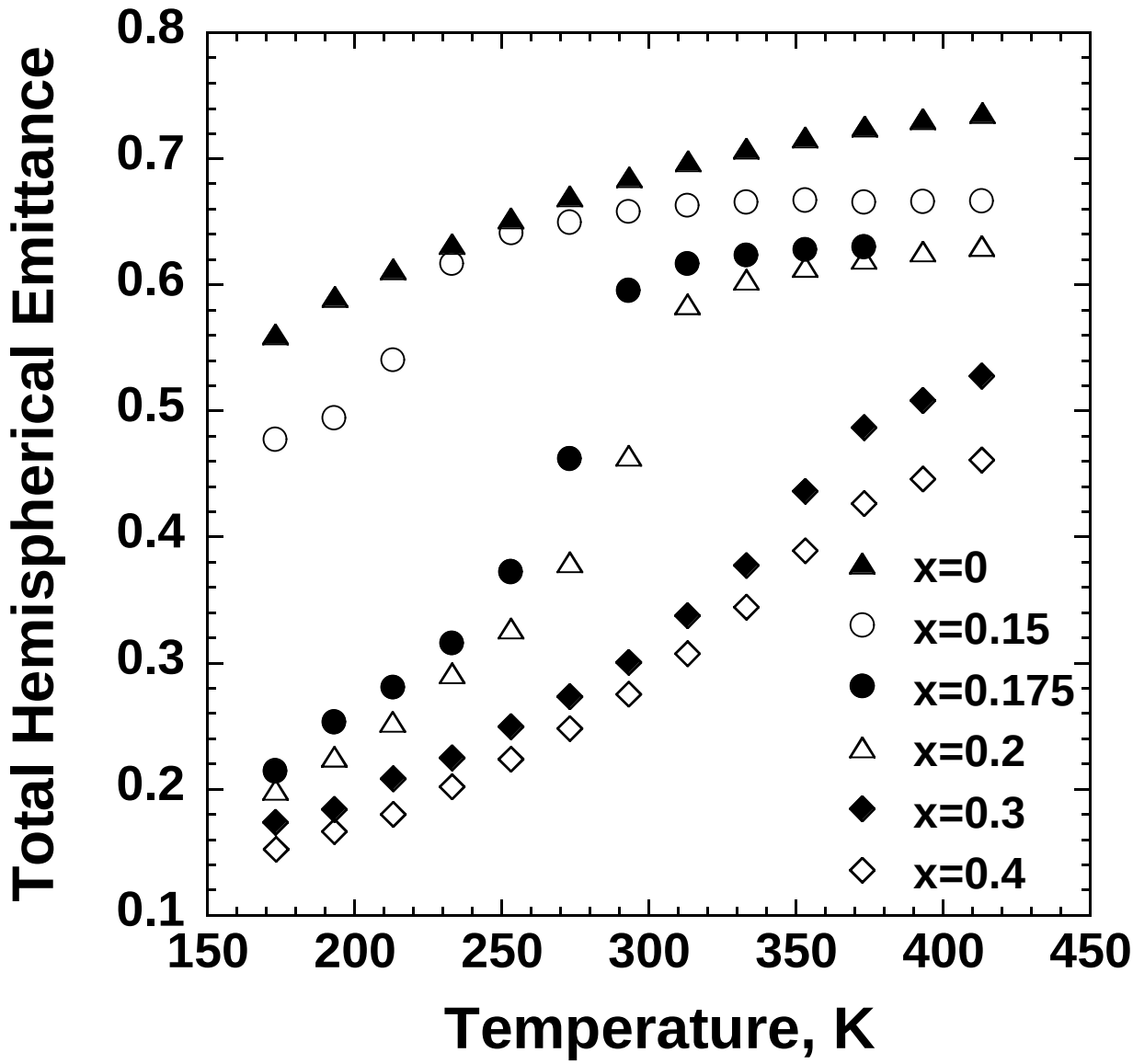
Total Hemispherical Emittance
0.8
0.7
0.6
0.5
0.4
0.3
0.2
0.1
150
200
250
300
350
400
450
Temperature, K
x=0
x=0.15
x=0.175
x=0.2
x=0.3
x=0.4

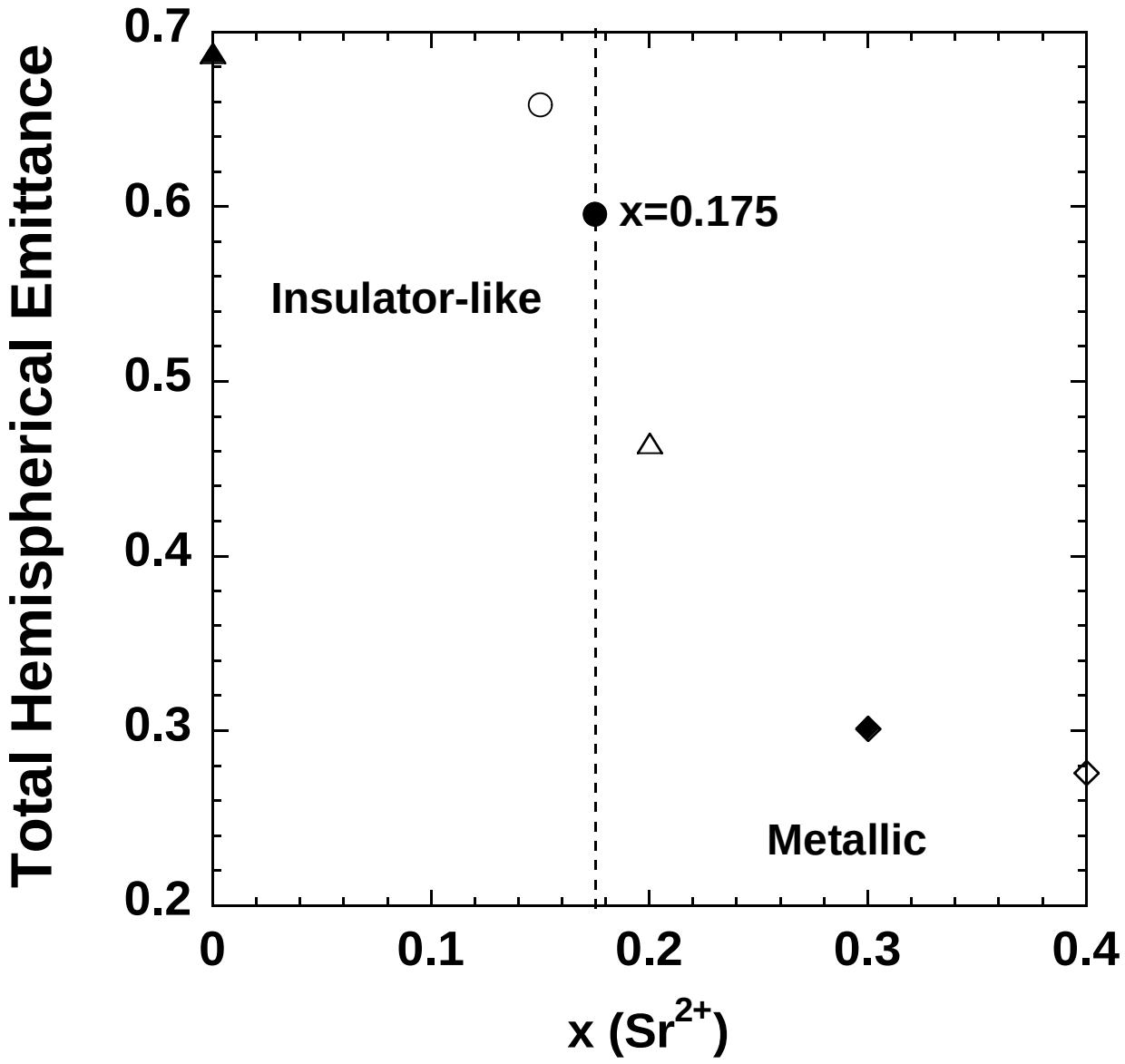
Total Hemispherical Emittance
0.7
0.6
0.5
0.4
0.3
0.2
0
0.1
0.2
0.3
0.4
x (Sr2+)
x=0.175
Insulator-like
Metallic

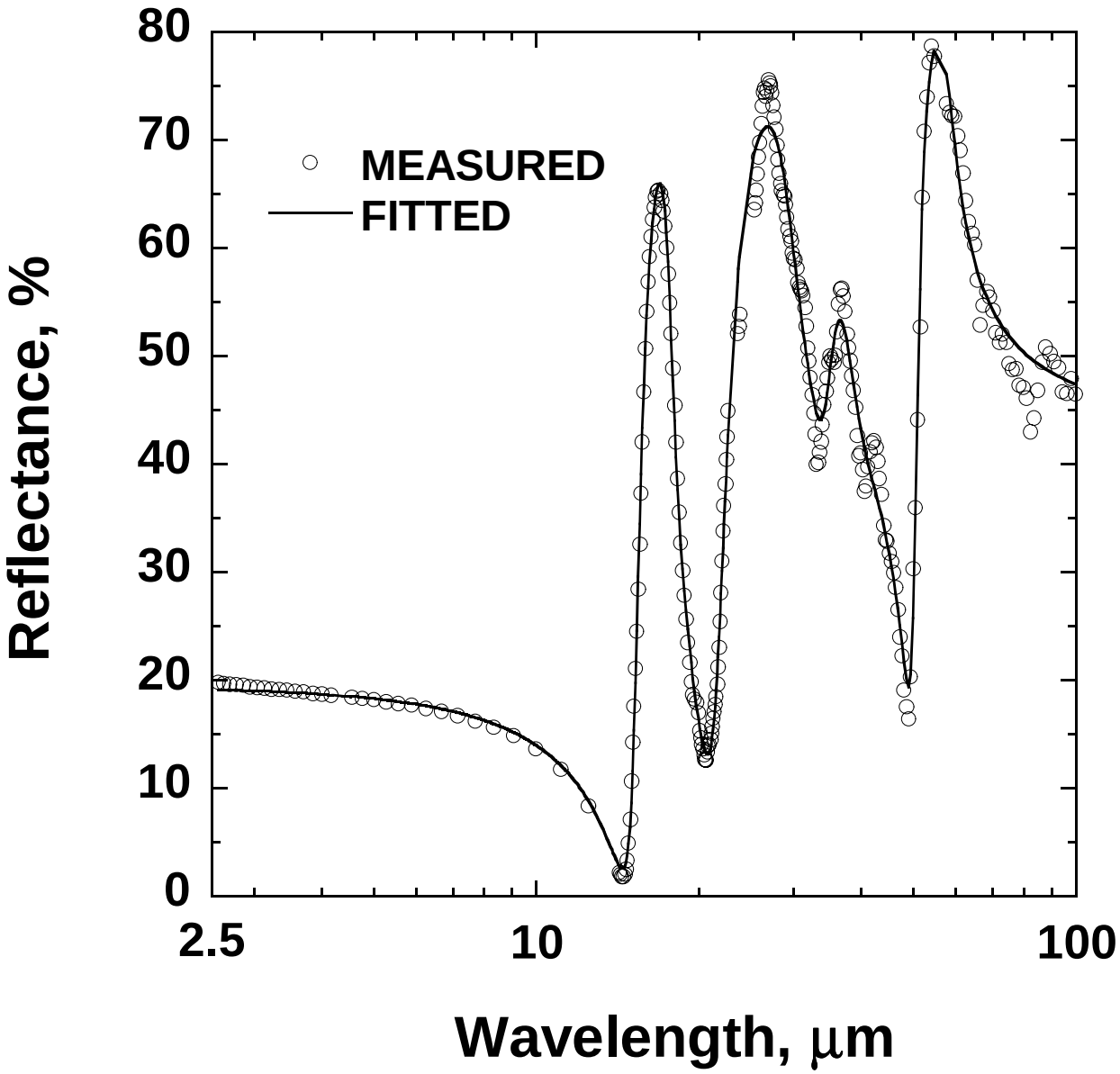
80
70
60
50
40
30
20
10
0
MEASURED
FITTED
Reflectance, %
2.5
10
100
Wavelength, μm

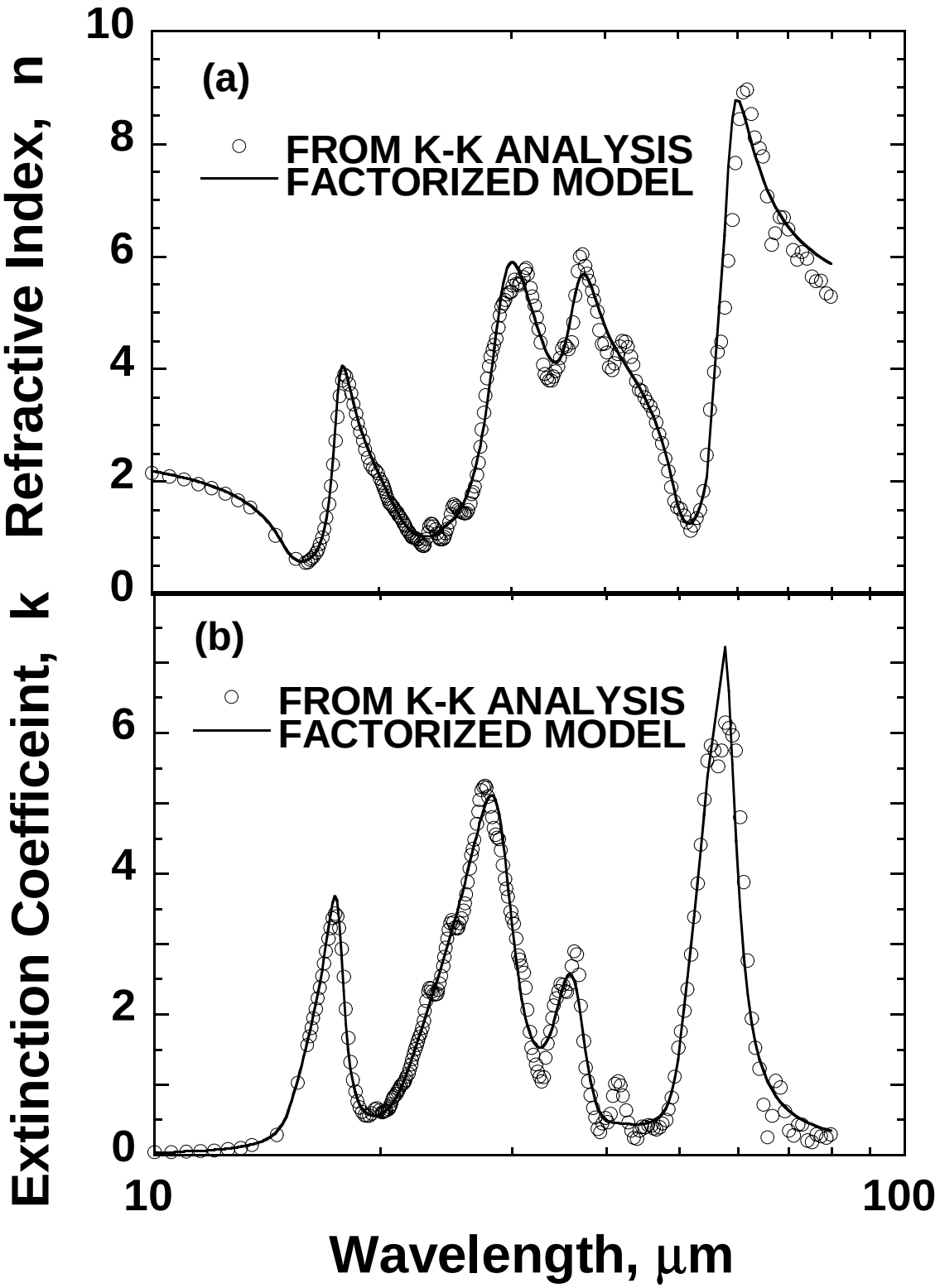
(a)
FROM K-K ANALYSIS
FACTORIZED MODEL
(b)
FROM K-K ANALYSIS
FACTORIZED MODEL
Extinction Coefficeint, k Refractive Index, n
Wavelength, μm
0
2
4
6
8
10
10
100

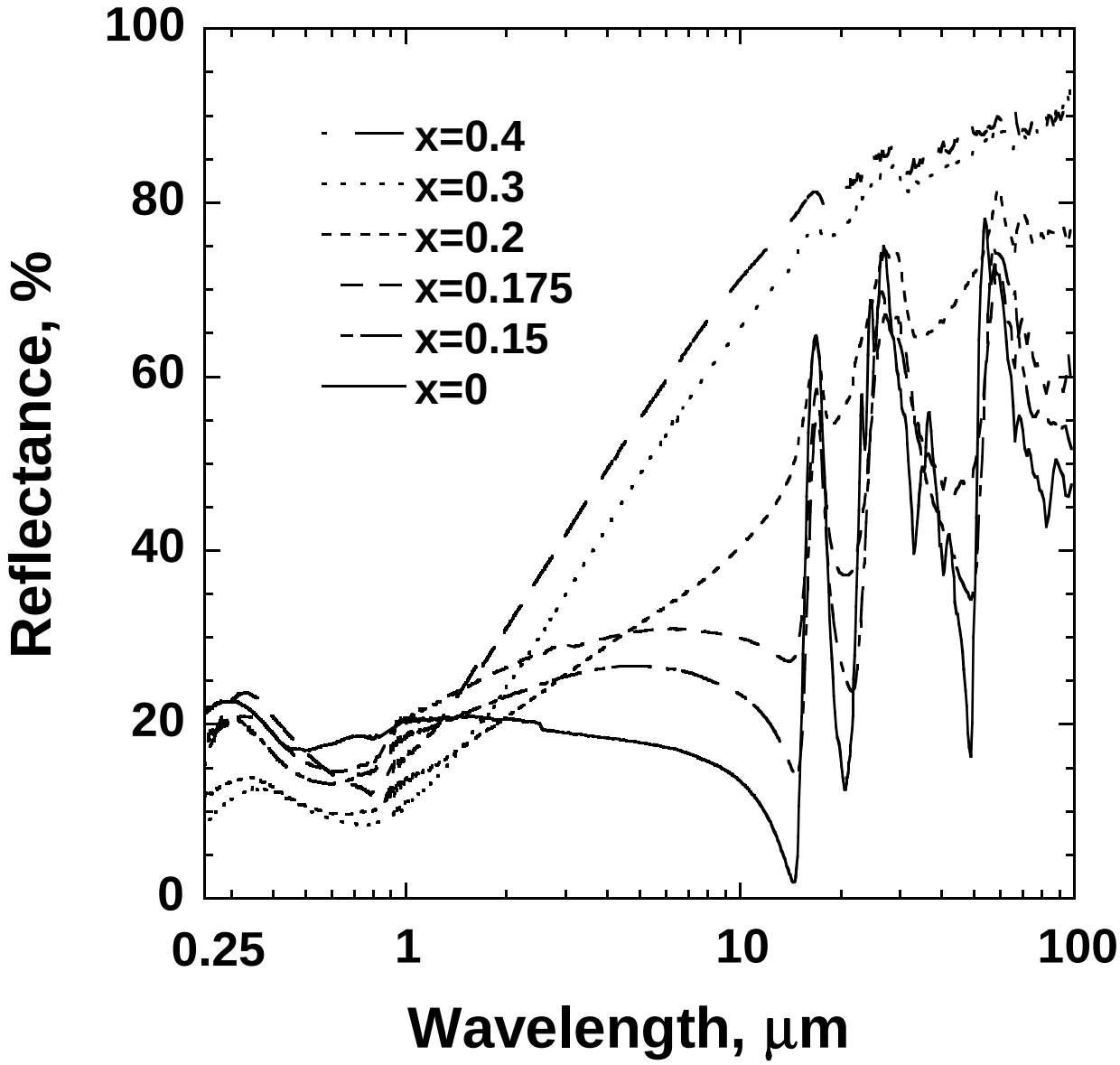
100
80
60
40
20
0
Reflectance, %
0.25
1
10
100
Wavelength, μm
x=0.4
x=0.3
x=0.2
x=0.175
x=0.15
x=0

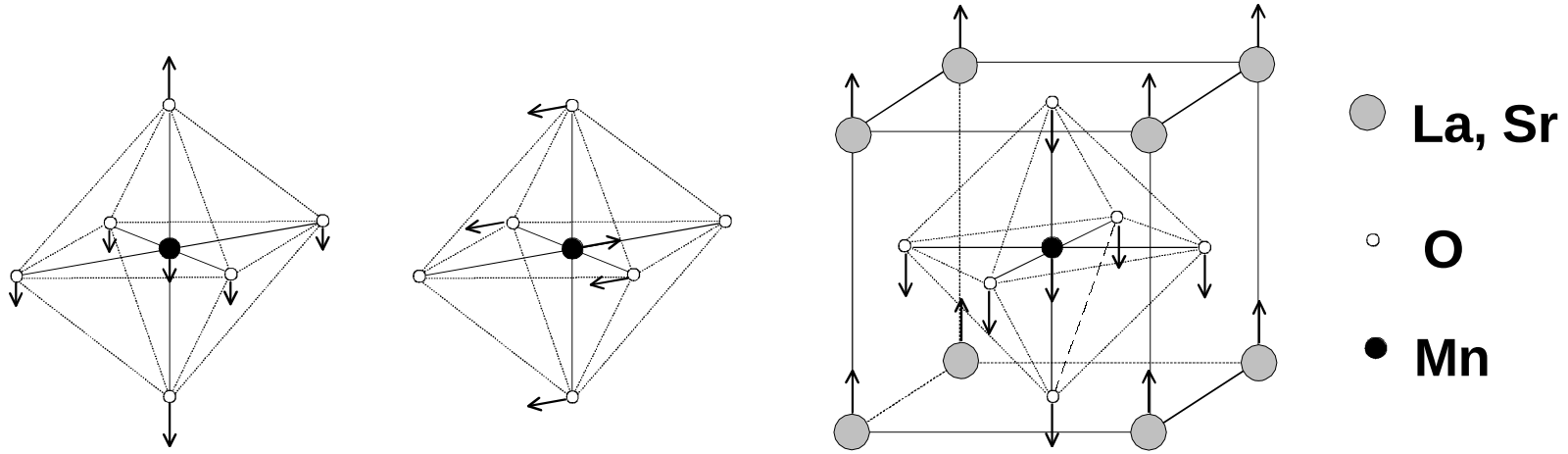

stretching mode **bending mode** **external mode**

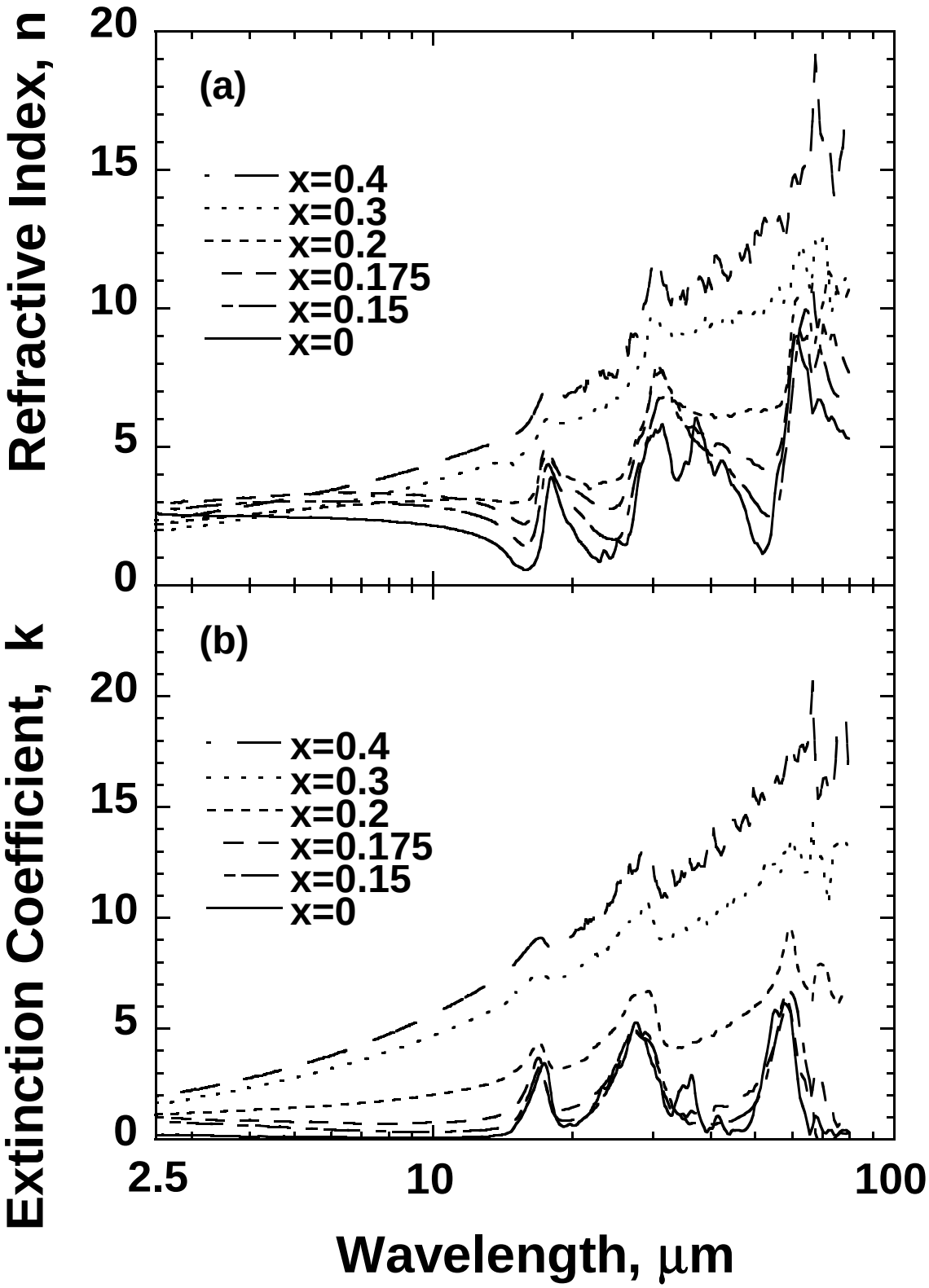
Refractive Index, n
Extinction Coefficient, k
(a)
(b)
x=0.4
x=0.3
x=0.2
x=0.175
x=0.15
x=0
0
5
10
15
20
2.5
10
100
Wavelength, μm

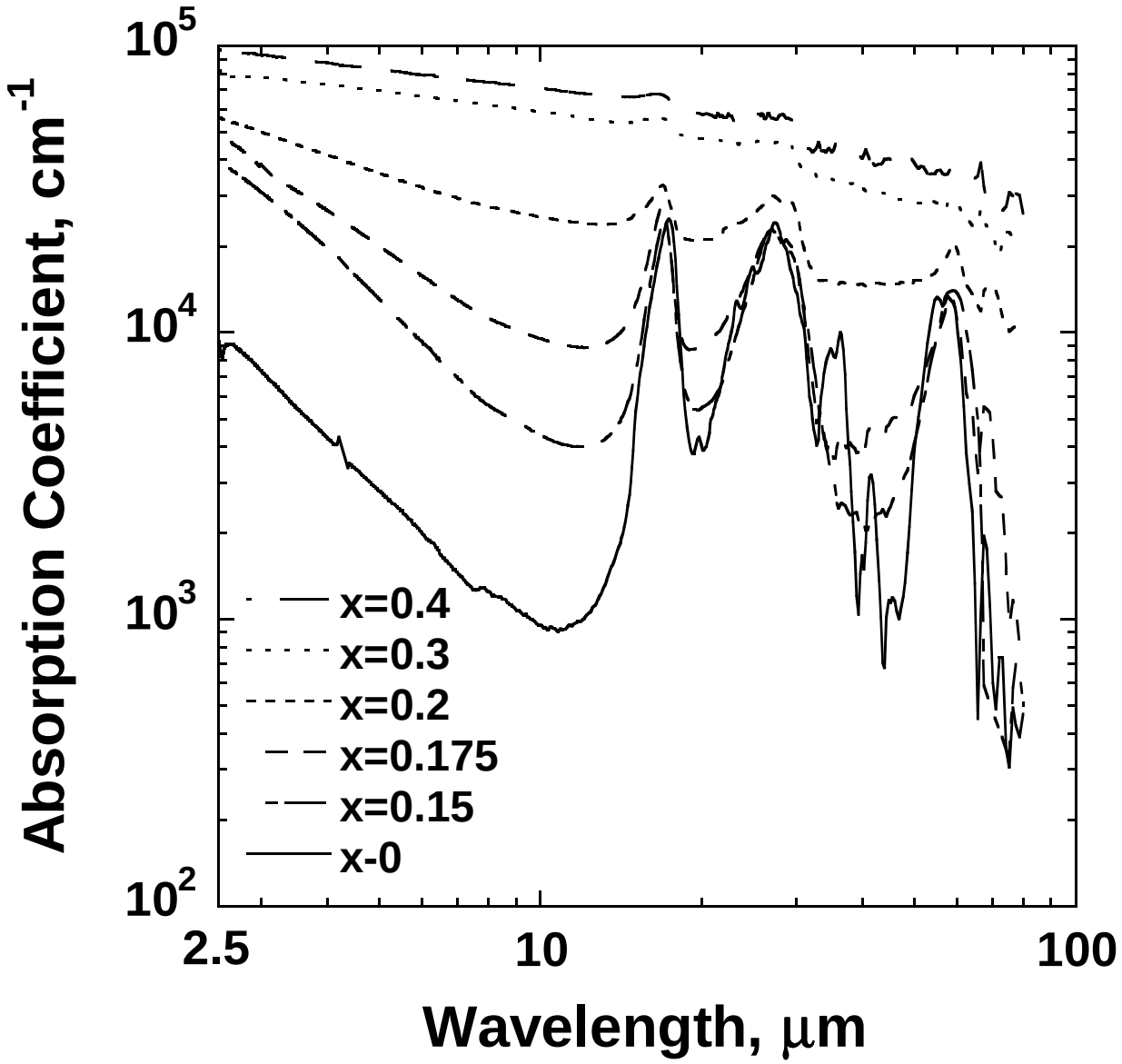
Absorption Coefficient, cm-1
10^5
10^4
10^3
10^2
2.5
10
100
Wavelength, μm
x=0.4
x=0.3
x=0.2
x=0.175
x=0.15
x-0